

The phenomenological MSSM in view of the 125 GeV Higgs data

B. Dumont^{a*}, J. F. Gunion^{b†}, S. Kraml^{a‡},

^a *Laboratoire de Physique Subatomique et de Cosmologie, UJF Grenoble 1,
CNRS/IN2P3, INPG, 53 Av. des Martyrs, F-38026 Grenoble, France*

^b *Department of Physics, University of California, Davis, CA 95616, USA*

Abstract

The parameter space of the phenomenological MSSM (pMSSM) is explored by means of Markov Chain Monte Carlo (MCMC) methods, taking into account the latest LHC results on the Higgs signal at 125 GeV in addition to relevant low-energy observables and LEP constraints. We use a Bayesian approach to derive posterior densities for the parameters and observables of interests. We find in particular that the Higgs measurements have a significant impact on the parameters μ and $\tan\beta$ due to radiative corrections to the bottom Yukawa coupling. We show moreover the impact of the most recent dark matter measurements on the probability distributions, and we discuss prospects for the next run of the LHC at 13–14 TeV.

*Email: dumont@lpsc.in2p3.fr

†Email: jfgunion@ucdavis.edu

‡Email: sabine.kraml@lpsc.in2p3.fr

1 Introduction

The recent discovery [1,2] of a new particle with mass of 125 GeV and properties consistent with the Standard Model (SM) Higgs boson is clearly the most significant news from the Large Hadron Collider (LHC). Thanks to the various production and decay modes that are accessible for such a light Higgs, and thanks to the excellent LHC operation, many complementary measurements of signal strengths, defined as $\mu \equiv (\sigma \times \text{BR})/(\sigma \times \text{BR})_{\text{SM}}$ for each production \times decay mode, are available from the 7–8 TeV LHC run [3–5]. These make it possible to determine the properties of the observed new state with good precision (see [6] for a global fit to the latest data).

So the Higgs has been found—but where is new physics? Indeed, the other significant news from the LHC is, unfortunately, the absence of any compelling sign of new physics. In particular, there is no hint of supersymmetry (SUSY), one of the most thoroughly studied ideas for physics beyond the SM (see, for example, Refs. [7,8] for recent reviews).

As is well known, in the Minimal Supersymmetric Standard Model (MSSM) a light Higgs mass of the order of 125 GeV requires that stops be either very heavy or near-maximally mixed. In addition to a modification of the electroweak symmetry breaking (EWSB) sector by the presence of a second Higgs doublet, the MSSM predicts a wealth of new particles that couple to the light Higgs boson. These can, depending on their masses and mixings, modify the Higgs couplings and consequently the production and decay rates of the Higgs boson in various channels. It is thus interesting to ask whether, besides the measured Higgs mass, the Higgs *signal strengths* provide constraints on the MSSM and may thus be used as a guide for where to look for SUSY.

Indeed, the apparent excess in the diphoton channel reported by both ATLAS and CMS in 2012 [1,2] motivated scenarios with light staus in the MSSM [9] or small $\tan\beta$ /large λ in the next-to-MSSM [10,11] (see also [12,13]). This drastically changed with the updated results presented at the Moriond 2013 conference and thereafter, which point towards a very SM-like Higgs boson, without the need of any modifications of the couplings due to new, beyond-the-SM particles.

The implications of the latest Higgs data for the MSSM were discussed recently in [14,15]. Ref. [14] concentrated on describing (the consequences for) the heavy Higgs states in the limit of heavy SUSY particles; the best coupling fit was found at low $\tan\beta$, $\tan\beta \approx 1$, with a not too high CP-odd Higgs mass of $m_A \approx 560$ GeV. Ref. [15] analyzed the consequences of the SUSY null-searches on the one hand and of the measurements of the Higgs properties on the other hand based on flat random scans of the so-called phenomenological MSSM (pMSSM) with the conclusion that SUSY searches and Higgs boson properties are to a very good approximation orthogonal. More concretely, Ref. [15] concluded that Higgs coupling measurements at the

14 TeV LHC, and particularly at a 500 GeV ILC, will be sensitive to regions of the pMSSM space that are not accessible to direct SUSY searches.

In this paper, we follow a different approach. Performing a Bayesian analysis of the pMSSM parameter space by means of a Markov Chain Monte Carlo analysis, we investigate how the latest LHC results on the properties of the 125 GeV Higgs state impact the probability distributions of the pMSSM parameters, masses and other observables. In doing so, we carefully take into account all available information on the production \times decay processes¹ on top of constraints from LEP searches and low-energy observables. In addition, we explore consequences for our probability distributions from the latest dark matter constraints and discuss prospects for measurements of the Higgs signal at the next run of the LHC at 13–14 TeV. Our results are orthogonal and directly comparable to the pMSSM interpretation of the CMS SUSY searches [18, 19].

2 Analysis

2.1 Definition of the phenomenological MSSM (pMSSM)

The purpose of this study is to assess what current Higgs data tell us, and do not tell us, about the MSSM at the weak scale, without any assumption as to the SUSY-breaking scheme. A priori, the weak-scale MSSM has 120 free parameters, assuming that R -parity is conserved (to avoid proton decay and to ensure that the lightest SUSY particle, the lightest supersymmetric particle (LSP), is stable) and assuming that the gravitino is heavy. This is clearly too much for any phenomenological study. However, most of these parameters are associated with CP-violating phases and/or flavor changing neutral currents (FCNC), which are severely constrained by experiment. A few reasonable assumptions about the flavor and CP structure therefore allow us to reduce the number of free parameters by a factor 6, without imposing any SUSY-breaking scheme. Working with parameters defined at the weak scale is indeed of great advantage for our purpose, because models of SUSY breaking always introduce relations between the soft terms that need not hold in general.

Concretely, the only generic way to satisfy very strong constraints on CP violation is to take all parameters to be real. FCNC constraints are satisfied in a generic way by taking all sfermion mass matrices and trilinear couplings to be flavor-diagonal. As a further simplification, the various independent sfermion masses for the 2nd generation are taken to be equal to their counterparts for the 1st generation. Regarding the trilinear A -terms of the first two generations, these only enter phenomenology multiplied by the associated very small Yukawa couplings

¹The importance of considering the distinct production \times decay processes—instead of just the decay modes—was recently emphasized in [16, 17].

and are thus not experimentally relevant unless unreasonably large. Only the 3rd generation parameters A_t , A_b and A_τ have observational impact.

This leaves us with 19 real, weak-scale SUSY Lagrangian parameters—the so-called p(henomenological) MSSM [20]. As mentioned, the pMSSM captures most of the phenomenological features of the R-parity conserving MSSM and, most importantly, encompasses and goes beyond a broad range of more constrained SUSY models. The free parameters of the pMSSM are the following:

- the gaugino mass parameters M_1 , M_2 , and M_3 ;
- the ratio of the Higgs vacuum expectation values (VEVs), $\tan \beta = v_2/v_1$;
- the higgsino mass parameter μ and the pseudo-scalar Higgs mass m_A ;
- 10 sfermion mass parameters $m_{\tilde{F}}$, where $\tilde{F} = \tilde{Q}_1, \tilde{U}_1, \tilde{D}_1, \tilde{L}_1, \tilde{E}_1, \tilde{Q}_3, \tilde{U}_3, \tilde{D}_3, \tilde{L}_3, \tilde{E}_3$ (with 2nd generation sfermion masses equal to their 1st generation counterparts, *i.e.* $m_{\tilde{Q}_1} \equiv m_{\tilde{Q}_2}$, $m_{\tilde{L}_1} \equiv m_{\tilde{L}_2}$, *etc.*), and
- the trilinear couplings A_t , A_b and A_τ ,

in addition to the SM parameters. To minimize theoretical uncertainties in the Higgs sector, these parameters are conveniently defined at the scale $M_{\text{SUSY}} \equiv \sqrt{m_{\tilde{t}_1} m_{\tilde{t}_2}}$, often also referred to as the EWSB scale.

The pMSSM parameter space is constrained by a number of theoretical requirements. In particular, the Higgs potential must be bounded from below and lead to consistent EWSB, and the sparticle spectrum must be free of tachyons. Moreover, in this study, we require that the LSP is the lightest neutralino, $\tilde{\chi}_1^0$. These requirements we refer to as theoretical constraints. Note that we do not check for charge and/or color breaking minima beyond warnings from the spectrum generator; this could be done, *e.g.*, using `Vevacious` [21], but would require too much CPU time for this study.

2.2 Construction of the pMSSM prior

We perform a global Bayesian analysis that yields posterior probability densities of model parameters, masses and observables. We allow the pMSSM parameters to vary within the following ranges:

$$\begin{aligned}
 -3 \text{ TeV} &\leq M_1, M_2, \mu \leq 3 \text{ TeV}; \\
 0 &\leq M_3, m_{\tilde{F}}, m_A \leq 3 \text{ TeV}; \\
 -7 \text{ TeV} &\leq A_t, A_b, A_\tau \leq 7 \text{ TeV}; \\
 2 &\leq \tan \beta \leq 60.
 \end{aligned} \tag{1}$$

A point in this space will be denoted by θ . In addition, we treat the SM parameters m_t , $m_b(m_b)$ and $\alpha_s(M_Z)$ as nuisance parameters, constrained with a likelihood. For each pMSSM point, we use `SoftSUSY_3.3.1` [22] to compute the SUSY spectrum, `SuperIso_v3.3` [23] to compute the low-energy constraints, and `micrOMEGAs_2.4.5` [24] to compute the neutralino relic density $\Omega_{\tilde{\chi}_1^0} h^2$, direct detection cross sections and to check compatibility with various pre-LHC sparticle mass limits. Moreover, we use `SDECAY_1.3b` [25] and `HDECAY_5.11` [26] to produce SUSY and Higgs decay tables. The various codes are interfaced using the SUSY Les Houches Accord [27].

The posterior density of θ given data D is given by

$$p(\theta|D) \sim L(D|\theta) p_0(\theta), \quad (2)$$

where $L(D|\theta)$ is the likelihood and $p_0(\theta)$ is the prior probability density, or prior for short. Beginning with a flat distribution in the parameters within the ranges defined by Eq. (1), $p_0(\theta)$ is obtained by incorporating the theoretical constraints noted above. In other words, $p_0(\theta)$ is the result of sculpting the flat parameter distributions by the requirements related to theoretical consistency and $\tilde{\chi}_1^0$ being the LSP. This $p_0(\theta)$ defines the starting prior, which will be modified by actual data using Eq. (2). Since we consider multiple independent measurements D_i , the combined likelihood is given by $L(D|\theta) = \prod_i L(D_i|\theta)$.

We partition the data into two parts:

1. a set of constraints, listed in Table 1, which are independent of the Higgs measurements; these constraints are used for the MCMC sampling and are collectively referred to by the label “preHiggs”, and
2. the Higgs measurements, which include the Higgs mass window, $m_h = 123 - 128$ GeV, and the signal strength likelihood as derived in [6].

With this partitioning, the posterior density becomes

$$p(\theta|D) \sim L(D^{\text{Higgs}}|\theta) L(D^{\text{preHiggs}}|\theta) p_0(\theta) = L(D^{\text{Higgs}}|\theta) p^{\text{preHiggs}}(\theta), \quad (3)$$

where $p_0(\theta)$ is the prior (as defined earlier) at the start of the inference chain and $p^{\text{preHiggs}}(\theta) \sim L(D^{\text{preHiggs}}|\theta) p_0(\theta)$ can be viewed as a prior that encodes the information from the preHiggs-measurements as well as the theoretical consistency requirements. This partitioning allows us to assess the impact of the Higgs results on the pMSSM parameter space while being consistent with constraints from the previous measurements. Note that at this stage we do not consider the direct limits from SUSY searches from ATLAS or CMS.

In addition to the experimental results included in our calculation of the prior $p^{\text{preHiggs}}(\theta)$, Table 1 lists the corresponding likelihood $L(D_j^{\text{preHiggs}}|\mu_j(\theta))$ for each observable j , where $\mu_j(\theta)$ denotes the model prediction for the observable j , such as $\text{BR}(b \rightarrow s\gamma)$ for a given θ . We obtained a discrete representation of the prior $p^{\text{preHiggs}}(\theta)$ within the sub-space defined in Eq. (1)

Table 1: The measurements that are the basis of our pMSSM prior $p^{\text{preHiggs}}(\theta)$. All measurements were used to sample points from the pMSSM parameter space via MCMC methods. The likelihood for each point was reweighted post-MCMC based on better determinations of $\text{BR}(b \rightarrow s\gamma)$, $\text{BR}(B_s \rightarrow \mu\mu)$, $R(B_u \rightarrow \tau\nu)$, and m_t .

i	Observable $\mu_j(\theta)$	Constraint D_j^{preHiggs}	Likelihood function $L(D_j^{\text{preHiggs}} \mu_j(\theta))$	MCMC / post-MCMC
1a	$\text{BR}(b \rightarrow s\gamma)$ [28, 29]	$(3.55 \pm 0.24^{\text{stat}} \pm 0.23^{\text{th}} \pm 0.09^{\text{sys}}) \times 10^{-4}$	Gaussian	MCMC
1b	$\text{BR}(b \rightarrow s\gamma)$ [30]	$(3.43 \pm 0.21^{\text{stat}} \pm 0.23^{\text{th}} \pm 0.07^{\text{sys}}) \times 10^{-4}$	Gaussian	reweight
2a	$\text{BR}(B_s \rightarrow \mu\mu)$ [31]	observed CL_s curve from [31]	$d(1 - \text{CL}_s)/d(\text{BR}(B_s \rightarrow \mu\mu))$	MCMC
2b	$\text{BR}(B_s \rightarrow \mu\mu)$ [32]	$(2.9 \pm 0.7 \pm 0.29^{\text{th}}) \times 10^{-9}$	Gaussian	reweight
3a	$R(B_u \rightarrow \tau\nu)$ [33]	1.63 ± 0.54	Gaussian	MCMC
3b	$R(B_u \rightarrow \tau\nu)$ [30]	1.04 ± 0.34	Gaussian	reweight
4	Δa_μ [34]	$(26.1 \pm 8.0^{\text{exp}} \pm 10.0^{\text{th}}) \times 10^{-10}$	Gaussian	MCMC
5a	m_t [35]	$173.3 \pm 0.5^{\text{stat}} \pm 1.3^{\text{sys}}$ GeV	Gaussian	MCMC
5b	m_t [36]	173.20 ± 0.87 GeV	Gaussian	reweight
6	$m_b(m_b)$ [33]	$4.19_{-0.06}^{+0.18}$ GeV	Two-sided Gaussian	MCMC
7	$\alpha_s(M_Z)$ [33]	0.1184 ± 0.0007	Gaussian	MCMC
8	particle masses	LEP [37] (via micrOMEGAs [24])	1 if allowed 0 if excluded	MCMC

by sampling points from $p^{\text{preHiggs}}(\theta)$ using a MCMC method (for an introduction see, *e.g.*, [38]). By construction, this method produces a sample of points whose density in the neighborhood of θ is $\propto p^{\text{preHiggs}}(\theta)$, *i.e.* the sampled points will constitute a discrete representation of the preHiggs likelihood as a function of the pMSSM parameters θ .

Our study is based on approximately 2×10^6 MCMC points, which were originally sampled for the CMS study [18] in which some of us participated. (The CMS study then used a random sub-sample of 7205 points from this data.) In the meanwhile, several experimental constraints that enter the preHiggs likelihood function have been updated. For example, first evidence for the decay $B_s \rightarrow \mu\mu$ was reported by the LHCb collaboration in [39] and recently new improved measurements have become available by CMS and LHCb [32]. We have taken the up-to-date value into account by reweighting each sampled point by the ratio of the new $\text{BR}(B_s \rightarrow \mu\mu)$ likelihood, 2b, to the old likelihood, 2a, in Table 1. Analogous reweighting was performed to take into account the updated values of $\text{BR}(b \rightarrow s\gamma)$, $R(B_u \rightarrow \tau\nu)$, and m_t .

2.3 Higgs likelihood

For fitting the properties of the observed Higgs boson, we use all the publicly available results on the signal strengths $\mu(X, Y)$ relative to SM expectations,²

$$\mu(X, Y) \equiv \frac{\sigma(X)\text{BR}(H \rightarrow Y)}{\sigma(X_{\text{SM}})\text{BR}(H_{\text{SM}} \rightarrow Y)}, \quad (4)$$

published by the ATLAS and CMS collaborations.³ Here, X denotes the fundamental production mechanisms: gluon fusion (ggF, $gg \rightarrow H$), vector-boson fusion (VBF, $WW/ZZ \rightarrow H$), and production in association with a Z or W boson (VH) or with a pair of top quarks (ttH); and Y denotes the Higgs decay final states ($Y = \gamma\gamma, ZZ^*, WW^*, b\bar{b}$ and $\tau\tau$ are currently accessible). Concretely, we consider the results in the (ggF+ttH) versus (VBF+VH) production plane for the $H \rightarrow \gamma\gamma, VV^* \equiv (ZZ^*, WW^*)$, and $\tau\tau$ decay modes. Moreover, we consider the results in the $b\bar{b}$ final state from vector boson associated production, as well as the ATLAS limits on invisible decays from ZH associated production with $Z \rightarrow \ell^+\ell^-$ and $H \rightarrow \text{invisible}$. All these results are combined into the ‘‘Higgs signal likelihood’’ $L(D^{\text{Higgs}}|\theta)$ in the form of $e^{-\chi_h^2/2}$, with the total χ^2 from the Higgs signal, χ_h^2 , computed using the global fitting program developed in [6]. (For details on the computation, we refer the interested reader to [6].)

For the concrete calculation, we use HDECAY_5.11 and approximate $\sigma(gg \rightarrow h)/\sigma(gg \rightarrow H_{\text{SM}}) \simeq \Gamma(h \rightarrow gg)/\Gamma(H_{\text{SM}} \rightarrow gg)$. Moreover, for computing the SM results entering Eq. (4), we use the MSSM decoupling limit with m_A and the relevant SUSY masses set to 4 TeV. This

²In the following, signals strengths are always denoted as $\mu(\text{process})$ in order to avoid confusion with the supersymmetric Higgs mass parameter, denoted as μ alone.

³Later the generic H of Eq. (4) will of course be the light MSSM Higgs, h .

ensures completely SM-like Higgs boson couplings at tree-level, as well as vanishing radiative contributions from the SUSY particles (including non-decoupling effects). We choose this procedure in order to guarantee that the radiative corrections being included are precisely the same for the numerator and denominator in Eq. (4).

For completeness, we also take into account the limits from the $H, A \rightarrow \tau\tau$ searches in the MSSM [40]. These limits are implemented in a binary fashion: we set the likelihood from each of these constraints to 1 when the 95% CL limit is obeyed and to 0 when it is violated. (Including or not including this limit however has hardly any visible effect on the posterior distributions.)

2.4 Dark matter constraints

The calculation of the properties of the neutralino LSP as a thermal cold dark matter (DM) candidate (or one of the cold DM components) depends on a number of cosmological assumptions, like complete thermalization, no non-thermal production, no late entropy production, *etc.* In order to be independent of these assumptions, we will show results with and without requiring consistence with DM constraints. When we do apply DM constraints, we adopt the following procedure. For the relic density, we apply an upper bound as a smoothed step function at the Planck value of $\Omega h^2 = 0.1189$ [41], accounting for a 10% theory-dominated uncertainty. Concretely, we take

$$L = \begin{cases} 1 & \text{if } \Omega h^2 < 0.119, \\ \exp[-((0.119 - \Omega h^2)/0.012)^2/2] & \text{if } \Omega h^2 > 0.119. \end{cases} \quad (5)$$

For the spin-independent scattering cross section off protons, we use the 90% CL limit from LUX [42], rescaling the computed $\sigma^{\text{SI}}(\tilde{\chi}_1^0 p)$ by a factor $\xi = \Omega_{\tilde{\chi}_1^0} h^2 / 0.119$ to account for the lower local density when the neutralino is only part of the DM. (The alternative would be to assume that the missing amount of $\Omega_{\tilde{\chi}_1^0} h^2$ is substituted by non-thermal production, which would make the direct detection constraints more severe. Our approach is more conservative in the sense of not being overly restrictive.)

2.5 Prompt chargino requirement

Before presenting the sampled distributions, another comment is in order. Letting M_1 , M_2 and μ , vary freely over the same range implies that about 2/3 of the time M_2 or μ will be the smallest mass parameter in the neutralino mass matrix. This implies that in a considerable portion of the pMSSM parameter space the $\tilde{\chi}_1^\pm$ and $\tilde{\chi}_2^0$ are close in mass or almost degenerate with the LSP, $\tilde{\chi}_1^0$ [43]. When the $\tilde{\chi}_1^\pm - \tilde{\chi}_1^0$ mass difference becomes very small, below about 300 MeV, the charginos are long-lived and can traverse the detector before they decay. This

typically occurs for wino-LSP scenarios with $|M_2| \ll |M_1|, |\mu|$. Since long-lived heavy charged particles were not considered in the SUSY searches used in [18], charginos were required to decay promptly; in practice this means a cut on the average proper lifetime of $c\tau < 10$ mm. In order to be able to directly compare our results (based on the Higgs measurements) with the CMS study (based on SUSY search results) [18] and its up-coming update [19], we also require “prompt” chargino decays, *i.e.* $c\tau < 10$ mm. Most of our conclusions are insensitive to this requirement. Wherever it matters, we will however also show the results obtained without imposing the $c\tau$ cut.

3 Results

3.1 Pre-Higgs distributions and impact of the Higgs mass

We begin our discussion by showing in Fig. 1 the sampled distributions of selected parameters and masses and the effect of the model prior. All distributions except that of the pMSSM prior $p_0(\theta)$ include the prompt chargino requirement; as can be seen, this requirement substantially alters the probability distributions for the parameters M_1 , M_2 , and μ and the chargino and neutralino masses relative to the $p_0(\theta)$ distributions, but has very little impact on the other parameters or masses. Further, in all the plots we observe that the preHiggs measurements incorporated in the MCMC influence the probability distributions relative to the simple prompt-chargino-decay distributions quite significantly, in particular shifting the neutralino, chargino, gluino, and also the stop/sbottom masses to higher values.

Also shown is the impact of requiring, in addition, that the mass of the light h fall in the window $123 \text{ GeV} \leq m_h \leq 128 \text{ GeV}$. This Higgs mass constraint strongly affects the stop mixing parameter $X_t/M_{\text{SUSY}} \equiv (A_t - \mu/\tan\beta)/\sqrt{m_{\tilde{t}_1}m_{\tilde{t}_2}}$, whose distribution takes on a two-peak structure emphasizing larger absolute values. More precisely, values around $|X_t/M_{\text{SUSY}}| \approx 2$, *i.e.* large but not maximal stop mixing is preferred. (Maximal stop mixing would mean $|X_t/M_{\text{SUSY}}| = \sqrt{6}$; for a detailed discussion of the relation between $|X_t/M_{\text{SUSY}}|$ and m_h see, *e.g.*, [44,45]). It is interesting to note here that, in view of naturalness, the optimal stop mixing is indeed somewhat shy of maximal [46]. The optimal value is actually quite close to that which has the highest probability in the pMSSM context, despite the fact that no measure of naturalness is input into the pMSSM likelihood analyses. The Higgs mass window requirement also results in a shift of the \tilde{t}_1 mass distribution to slightly larger values; however, compared to the impact of the preHiggs constraints the effect is quite small. Aside from an increased preference for values of $\tan\beta \approx 10 - 20$, the other parameters and masses are hardly affected by the Higgs mass window.

It is also interesting to consider the h signal at this level. Some relevant distributions are

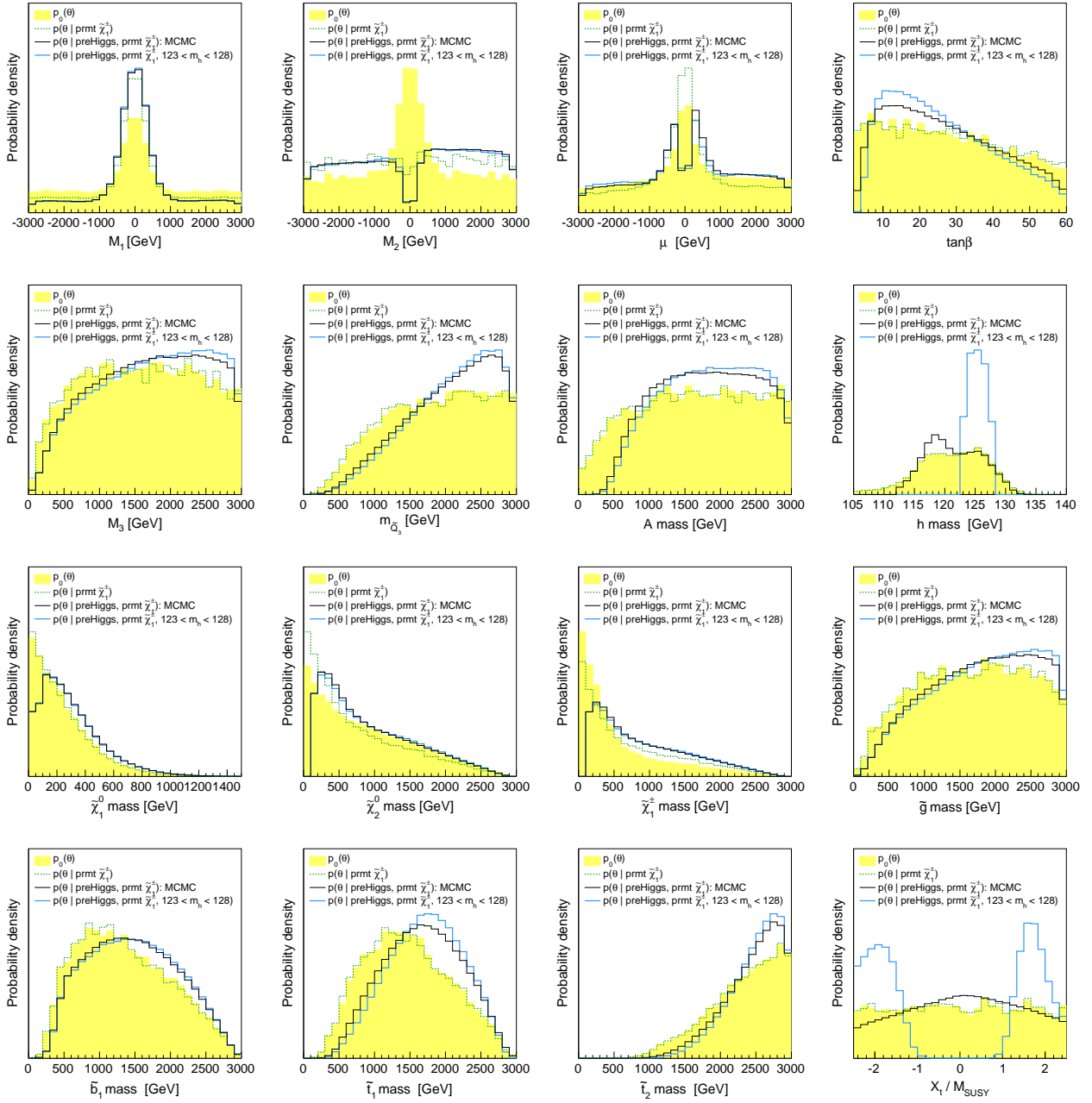


Figure 1: Marginalized 1D posterior densities for selected parameters and masses. The yellow histograms show the sampled distributions, $p_0(\theta)$, as obtained after imposing theoretical constraints starting from a flat scan in the parameter ranges specified by Eq. (1). The dashed green lines are the distributions after requiring prompt charginos (prmt), the full black lines show the distributions based on the “preHiggs” measurements of Table 1, and the full blue lines the ones when requiring $m_h = [123, 128]$ GeV in addition to “prmt” and “preHiggs” constraints. The bottom right plot of X_t/M_{SUSY} shows that large (but not maximal) stop mixing is favored by the $m_h = 123 - 128$ GeV requirement.

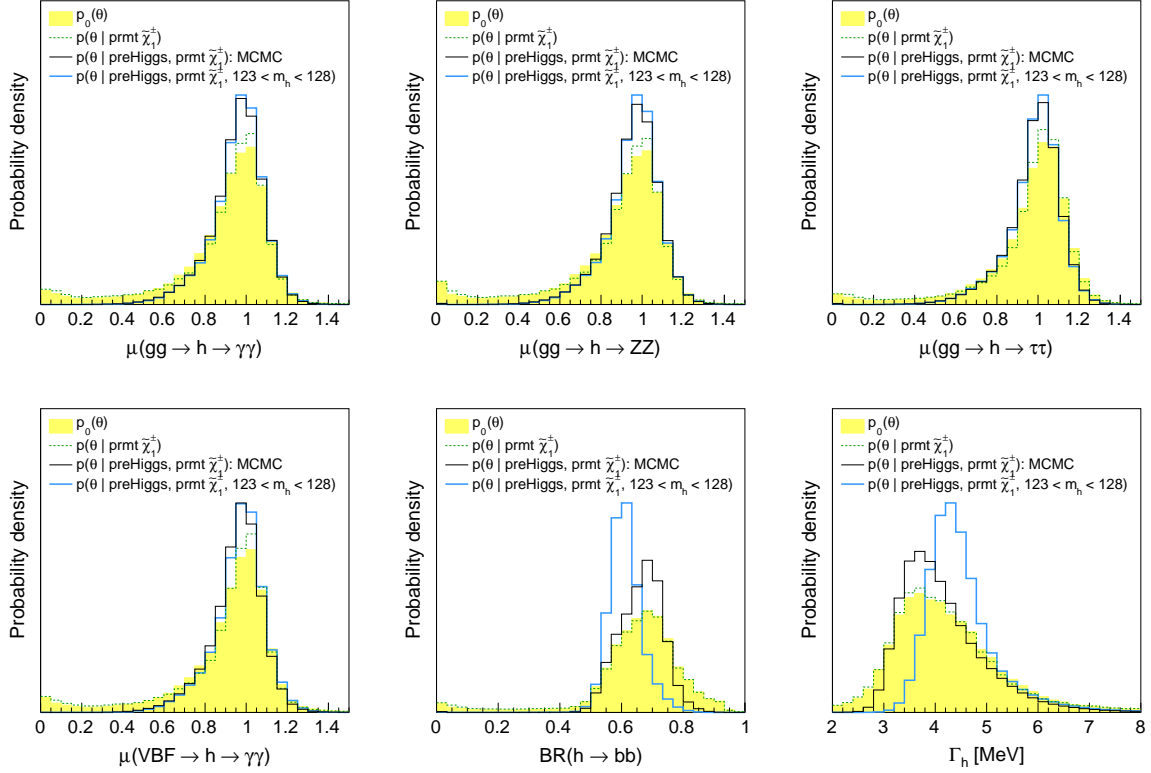


Figure 2: Same as Fig. 1 but for selected h signal strengths, $\text{BR}(h \rightarrow b\bar{b})$ and the total decay width Γ_h . The VBF distributions look practically the same as the ggF distributions, as exemplified for the VBF $\rightarrow h \rightarrow \gamma\gamma$ case, though they show a slightly larger effect from requiring $m_h = 123 - 128$ GeV than the ggF distributions.

shown in Fig. 2. While generically the h signal strength can go down to zero in the MSSM, already the “preHiggs” constraints eliminate very small values below $\mu \approx 0.6$ and narrow the signal strength distributions to a range of $\mu \approx 1 \pm 0.4$. This is coming from two different effects. First, in the low- m_A region the heavier scalar H can be more SM-like than h . Second, in the region where the LSP is light ($m_{\tilde{\chi}_1^0} \lesssim 65$ GeV) a large increase of the total width, resulting in reduced signal strengths, is possible through $h \rightarrow \tilde{\chi}_1^0 \tilde{\chi}_1^0$. The low- m_A region is mostly disfavored from flavor constraints, while a light neutralino—if mainly wino or higgsino—is excluded by the LEP bound on charginos. In both cases, requiring $m_h = 123 - 128$ GeV only has a very small additional effect.

One might expect that the influence of the Higgs mass is larger in the ggF channels than in the VBF channels (because of the negative loop contribution from maximally mixed stops affecting the former) but, in fact, the effect is very small and goes in the opposite direction, as can be seen by comparing the top-left and the bottom-left plots in Fig. 2. The observables

which are really influenced by the Higgs mass are the branching ratio into $b\bar{b}$, which becomes centered around $\text{BR}(h \rightarrow b\bar{b}) \approx 0.6$, and the h total width, for which the most likely value is shifted a bit upwards to $\Gamma_h \approx 4\text{--}5$ MeV. However, this is not really a SUSY effect: the same happens for the SM Higgs when going from $m_H \lesssim 120$ GeV to $m_H \approx 125$ GeV.

3.2 Impact of Higgs signal strengths

As the next step, we include in addition the detailed properties of the h signal in the computation of the likelihood as outlined in Section 2.3. The effects of the Higgs observations on the pMSSM parameters and on the particle masses are shown in Fig. 3. In these plots, the light blue histograms show the distributions based on the “preHiggs” measurements of Table 1 plus requiring in addition $m_h \in [123, 128]$ GeV, *i.e.* they correspond to the blue line-histograms of Fig. 1. The solid red lines are the distributions when moreover taking into account the measured Higgs signal strengths in the various channels as outlined in Section 2. Note that the limits from the MSSM $H, A \rightarrow \tau\tau$ searches, which are also included in the red line-histograms, have a negligible effect. (For completeness, a plot of the $\tan\beta$ versus m_A plane is given in Fig. 6.) Finally, the dashed red lines also take into account upper limits from the DM relic density and direct DM searches, as explained in Section 2.4.

Let us first discuss the effect of the Higgs measurements, *i.e.* consider the solid red lines only. We observe a significant preference for small or negative μ and smaller $\tan\beta$ values when including the Higgs signal strength likelihood. The main reason is the $\mu \tan\beta$ correction to the bottom Yukawa coupling [47, 48], which for large $\tan\beta$ and large positive (negative) μ enhances (reduces) $\Gamma(h \rightarrow b\bar{b})$ and the total h width, hence reducing (increasing) all signal strengths except $\mu(Vh \rightarrow b\bar{b})$. The preference for positive μ comes from the slight excess in the VBF and VH channels of $\gamma\gamma$ (mainly seen by ATLAS). In Ref. [6], $\mu(\text{VBF} + \text{VH}, \gamma\gamma) = 1.72 \pm 0.59$ is found, while other combined signal strengths are fully compatible with 1 at 68% CL. An overall excess (negative μ) is therefore preferred over a general deficit (positive μ). To a good approximation, the correction to the bottom Yukawa coupling is given by

$$\Delta_b \equiv \frac{\Delta m_b}{m_b} \simeq \left[\frac{2\alpha_s}{3\pi} \mu m_{\tilde{g}} I(m_{\tilde{g}}^2, m_{\tilde{b}_1}^2, m_{\tilde{b}_2}^2) + \frac{\lambda_t^2}{16\pi^2} A_t \mu I(\mu^2, m_{\tilde{t}_1}^2, m_{\tilde{t}_2}^2) \right] \tan\beta, \quad (6)$$

where $I(x, y, z)$ is of order $1/\max(x, y, z)$ [44]. The shifts to higher values of all four stops and sbottoms masses and to lower values for the gluino mass also come from Δ_b . In addition, negative values of A_t are more likely after taking into account the Higgs likelihood. This comes from the second term of Eq. (6): in order to compensate the first, dominant term, $\text{sgn}(A_t \mu) = -\text{sgn}(\mu)$ is required, hence a negative A_t . The tree-level coupling hbb also has an effect. It is given by

$$g_{hbb} \simeq 1 - \frac{M_Z^2}{2m_A^2} \sin 4\beta \tan\beta, \quad (7)$$

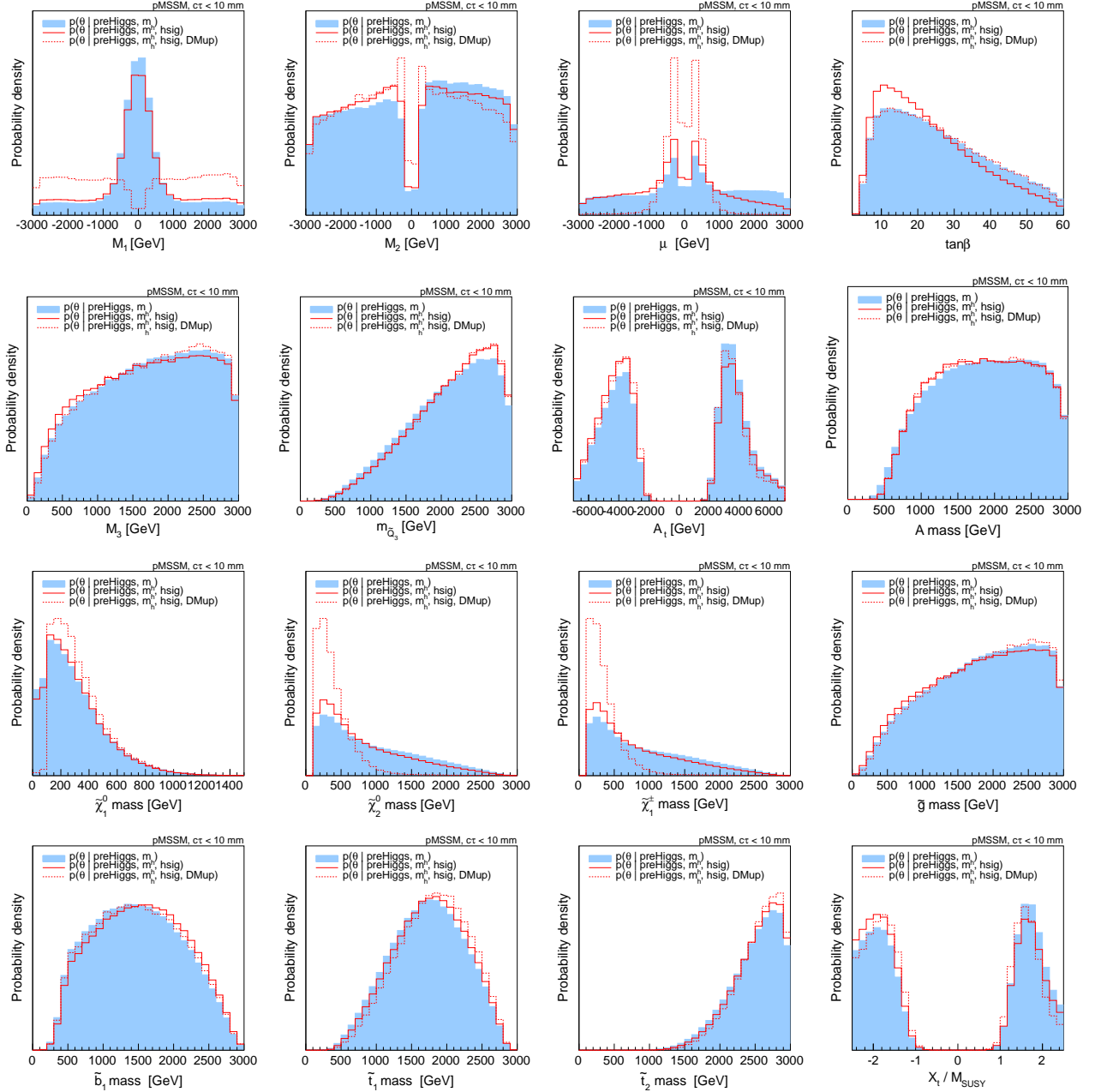


Figure 3: Marginalized 1D posterior densities for selected parameters and masses, showing the effect of the Higgs signal strength measurements. The light blue histograms show the distributions based on the “preHiggs” measurements of Table 1 plus requiring in addition $m_h \in [123, 128]$ GeV. The solid red lines, labelled “hsig”, are the distributions when moreover taking into account the measured Higgs signal strengths in the various channels. The limits from searches for the heavy Higgses (H and A) are also included in the red line-histograms, but have a totally negligible effect. The dashed red lines, labelled “DMup”, include in addition an upper limit on the neutralino relic density and the recent direct DM detection limit from LUX as explained in the text.

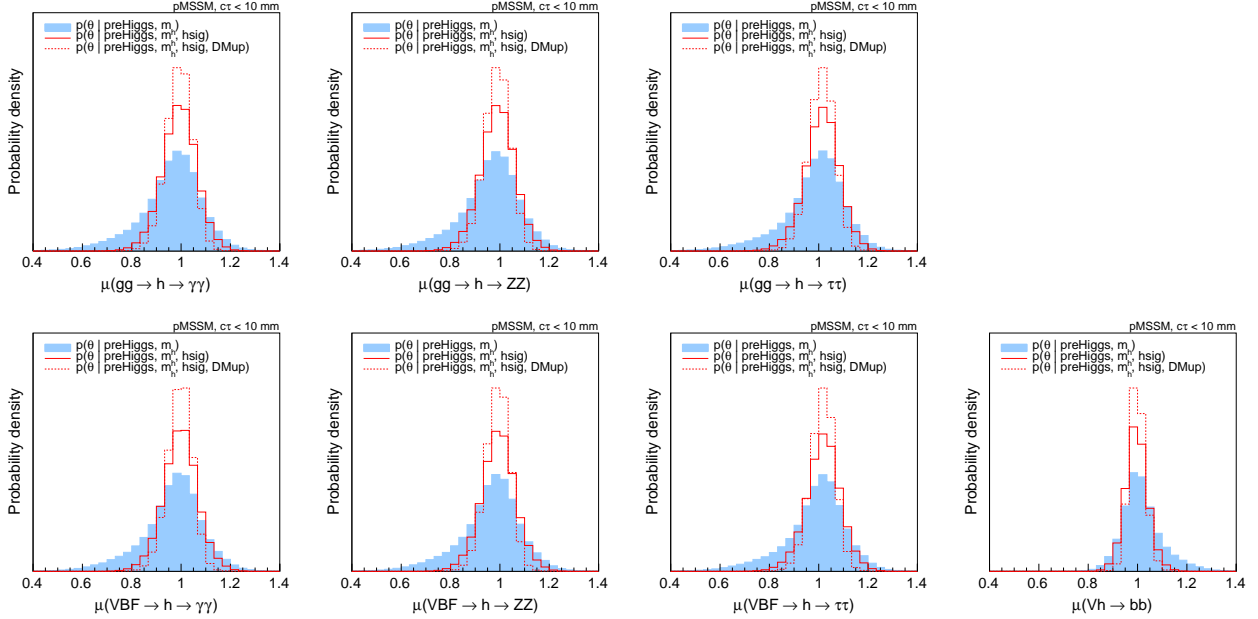


Figure 4: Same as Fig. 3 but for the relevant h signal strengths.

for $m_A \gg M_Z$ [44], and disfavors relatively light A and H , with masses below about 700 GeV (the effect from imposing the CMS $H, A \rightarrow \tau\tau$ limit is subdominant). Finally, M_2 shows a slight preference towards negative values. This is a direct consequence of the asymmetry in the distribution of μ , since $\text{sgn}(\mu M_2) > 0$ is required for $\Delta a_\mu^{\text{SUSY}} > 0$ as suggested by the data.

The DM constraints, on the other hand, have a dramatic effect on the bino and higgsino mass parameters and in turn on the chargino and neutralino masses. Since a mostly bino $\tilde{\chi}_1^0$ generically leads to a large $\Omega_{\tilde{\chi}_1^0} h^2$, low values of M_1 are strongly disfavored. The preferred solutions have a relevant higgsino or wino fraction of the LSP; therefore $\tilde{\chi}_1^\pm$ and $\tilde{\chi}_2^0$ masses below about 1 TeV are strongly favored. At the same time, very light LSP masses below about 100 GeV are severely limited because of the LEP bound on the chargino mass. The preferred value of $\tan\beta$ is also affected; in fact, the preference for lower $\tan\beta$ coming from the Higgs signal strengths is removed by the DM constraints. The reason for this is an enhancement of A -funnel annihilation to comply with the upper limit on $\Omega_{\tilde{\chi}_1^0} h^2$.

The posterior distributions of the h signal strengths in the various channels are shown in Fig. 4. The red line-histograms correspond of course to the constraints which we used as experimental input. For the $\gamma\gamma$, ZZ and $\tau\tau$ final states, we find signal strengths of about 1 ± 0.15 after the Higgs signal requirements, and about 1 ± 0.10 after the DM requirements, at 95% Bayesian Credibility (BC). For the $b\bar{b}$ final state, the distribution is much narrower than required by observations—we find that $\mu(Vh \rightarrow b\bar{b})$ is restricted to the 95% BC interval $\mu(Vh \rightarrow b\bar{b}) \in [0.91, 1.09]$ after Higgs signal requirements, and $[0.94, 1.06]$ after DM requirements. This

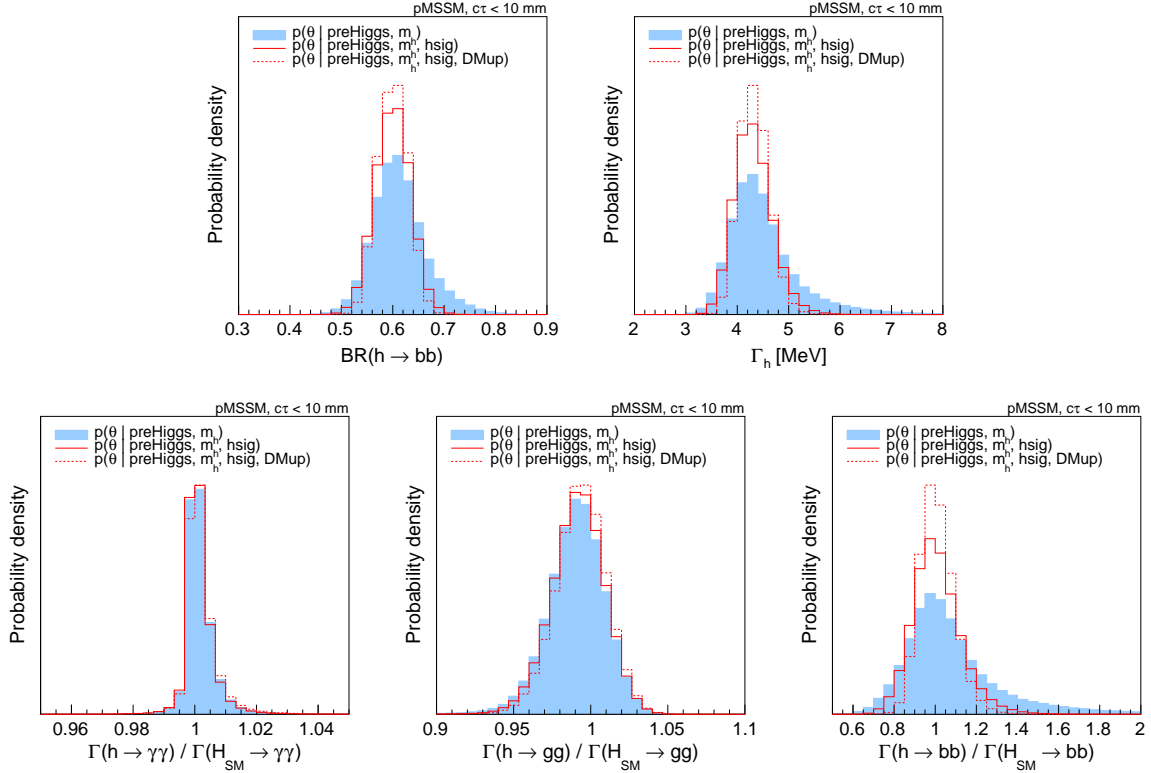


Figure 5: Marginalized 1D posterior densities as in Fig. 3, in the top row for $\text{BR}(h \rightarrow b\bar{b})$ and Γ_h , in the bottom row for $\Gamma(h \rightarrow Y)/\Gamma(H_{\text{SM}} \rightarrow Y)$ with, from left to right, $Y = \gamma\gamma$, gg and $b\bar{b}$.

is an indirect effect of the constraint on $\text{BR}(h \rightarrow b\bar{b})$ and the total h width, Γ_h , in order to have large enough signal in the other channels, see Fig. 5. Interestingly, the constraints from the DM side narrow the signal strength distributions even more around the SM value of 1 because the higgsino mass μ tends to take on small values to fulfill the relic density requirement, leading to smaller Δ_b .

Figure 5 also shows posterior distributions of $r_Y \equiv \Gamma(h \rightarrow Y)/\Gamma(H_{\text{SM}} \rightarrow Y)$ for $Y = \gamma\gamma$, gg and $b\bar{b}$. These ratios are equivalent to the ratios of the coupling strengths squared; $r_{\gamma\gamma} = C_\gamma^2$, $r_{gg} = C_g^2$, $r_{bb} = C_D^2$ in the notation of [6]. Our results for r_Y can be compared to those for the neutralino LSP case in Ref. [15]. We observe that in our case $r_{\gamma\gamma}$ peaks sharply at 1, the 95% BC interval being $[0.99, 1.01]$, while r_{gg} shows a wider distribution with a 95% BC interval of $[0.96, 1.02]$. (The picture does not change if we remove the $c\tau$ cut.). These features are different from those in [15], where the $r_{\gamma\gamma}$ distribution peaks within $r_{\gamma\gamma} \approx 1$ –1.05, and r_{gg} exhibits an upper limit of $r_{gg} \lesssim 0.97$. Also, the r_{bb} distribution is quite different. Some differences are of course expected as the distributions in [15] come from a flat random sampling and thus do not have the statistical meaning that underlies our approach. More importantly, however, the SM

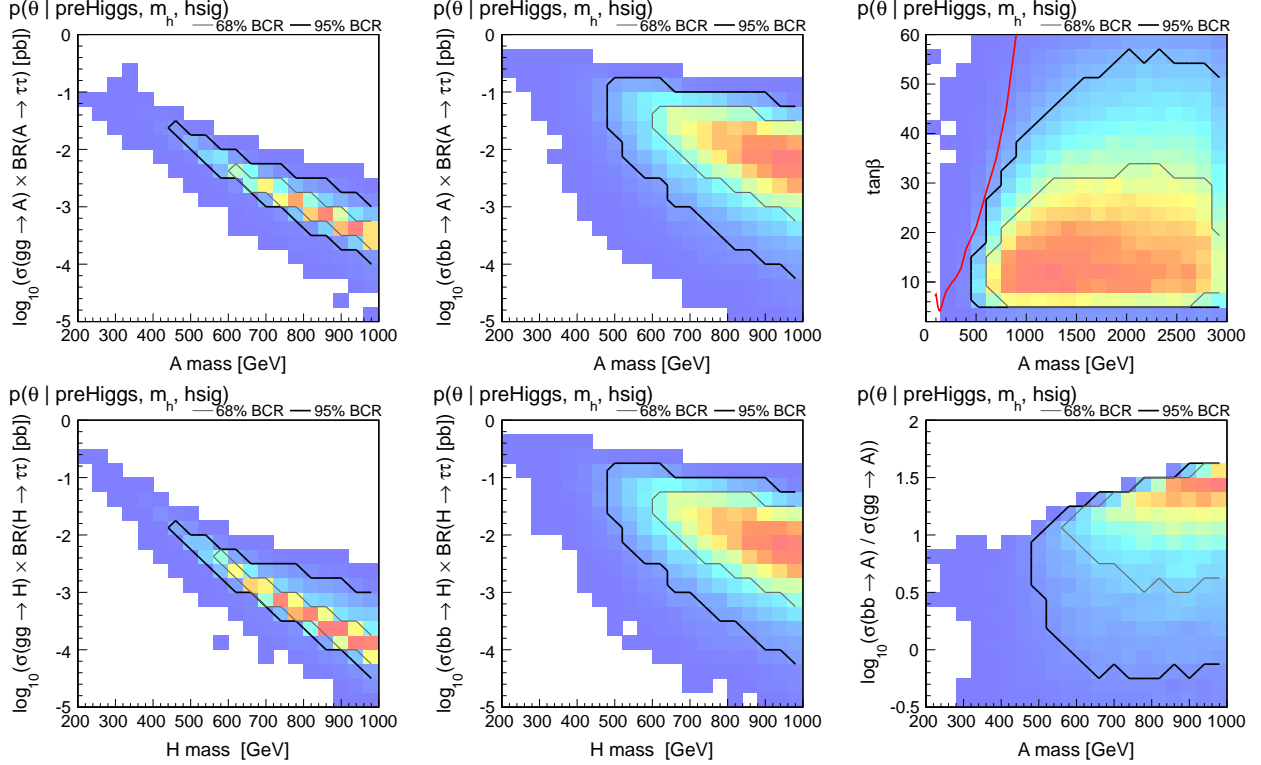


Figure 6: Marginalized posterior densities in 2D for the heavy MSSM Higgses A and H . The plots on the left and in the middle show $\sigma \times \text{BR}$ in the $\tau\tau$ final state, from bb and gg production at $\sqrt{s} = 14$ TeV, versus the A or H mass. The top-right plot shows the posterior density in the $\tan\beta$ versus m_A plane with the latest 95% CL from the CMS search for MSSM $H, A \rightarrow \tau\tau$ [40] superimposed. The bottom-right plot compares bb to gg production as function of m_A . In all plots, the probability density is represented by color shading, ranging from low values in blue to high values in red. The grey and black lines are contours of 68% and 95% Bayesian Credibility, respectively.

calculation of HDECAY employed in [15] includes additional radiative corrections which are not present in the MSSM calculation.⁴ In our case, we avoid this problem by taking the MSSM decoupling case as the SM limit for computing $\Gamma(H_{\text{SM}} \rightarrow Y)$, *cf.* Section 2.3. Of course, the r_Y are not directly measurable at the LHC. They become measurable only if it can be determined that the h has no invisible (*e.g.* $h \rightarrow \tilde{\chi}_1^0 \tilde{\chi}_1^0$) or unseen (*e.g.* $h \rightarrow 4\tau$) decay modes.

Our procedure also allows us to derive predictions for the heavier MSSM Higgs states H , A and H^\pm , as illustrated in Figs. 6 and 7. First, in the $\tan\beta$ versus m_A plane, we show that the current CMS limit [40] interpreted in the m_h^{max} scenario has a negligible effect on our distributions, since after imposing constraints from low-energy observables and from Higgs

⁴We thank Ahmed Ismail and Matthew Cahill-Rowley for communication on this matter.

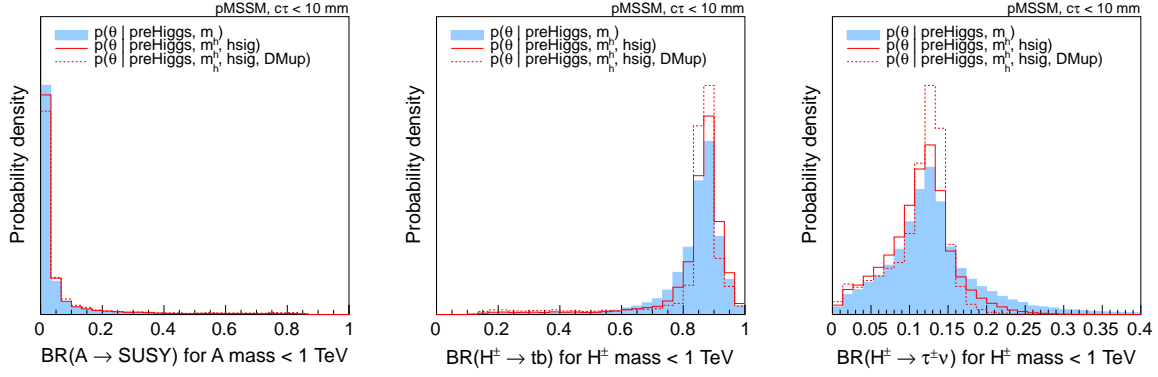


Figure 7: Marginalized 1D posterior densities as in Fig. 3, here for the branching ratios of the heavy MSSM Higgses A and H^\pm with masses below 1 TeV.

measurements the likely region corresponds to A masses above 500 GeV and moderate $\tan\beta$. (This observation remains valid when dark matter requirements are taken into account; in all cases we have checked that the current limits on $H \rightarrow ZZ$ are always satisfied.) We also show $\sigma(gg, b\bar{b} \rightarrow H, A) \times \text{BR}(H, A \rightarrow \tau\tau)$ at $\sqrt{s} = 14$ TeV as a function of $m_{H,A}$, using `SusHi_1.1.1` [49] for the computation of the cross sections in the approximation of decoupled stops and sbottoms.⁵ These plots show that the signals from the CP-odd and CP-even Higgs bosons are very similar and that for high masses the dominant process is almost always $b\bar{b} \rightarrow H, A$ (see, in particular, the bottom right plot), where for a given mass $\sigma(b\bar{b} \rightarrow H, A)$ spans over about an order of magnitude due to its strong dependence on $\tan\beta$. Typical $\sigma \times \text{BR}$ values are of the order of 0.1 to 100 fb for $m_{H,A} < 1$ TeV and therefore most of this region should be probed during the next run of the LHC at 13–14 TeV.

Some more properties of the heavy Higgses (for masses < 1 TeV) are shown in Fig. 7. We see that the decay branching fraction of A into SUSY particles is often very small because most of the supersymmetric partners generally lie at the (multi-)TeV scale. Concretely, the probability for $\text{BR}(A \rightarrow \text{SUSY}) > 10\%$ is only 1.6% after the Higgs signal likelihood (2.1% after DM requirement). Compared to the preHiggs distributions, decays into SUSY particles are however slightly enhanced by the Higgs likelihood and dark matter requirements because μ , and hence neutralino and chargino masses, are pushed to lower values. Also shown are the dominant decay modes of the charged Higgs: $H^\pm \rightarrow tb$ and $H^\pm \rightarrow \tau^\pm\nu$. The dominance of hadronic decays over leptonic ones is strengthened when Higgs measurements are taken into account since small values of m_A and large values of $\tan\beta$ are then disfavored.

⁵Neglecting contributions from stops and sbottoms in the computation of $gg, b\bar{b} \rightarrow H, A$ is a good approximation in most cases since the posterior densities of $m_{\tilde{t}_1}$ and $m_{\tilde{b}_1}$ peak around 2 TeV.

3.3 Impact of the $c\tau$ cut

We saw from the plots in Section 3.1 that the “prompt chargino” requirement has a strong effect on some of the distributions, above all on that of the wino mass parameter M_2 . The influence on μ and M_1 is less dramatic but still quite strong. As a consequence, it is mostly the chargino and neutralino masses (and their gaugino–higgsino composition) which are affected by the $c\tau < 10$ mm requirement. To assess the impact of this cut, the relevant posterior densities *without* the $c\tau$ cut are shown in Fig. 8. Comparing these plots with their equivalents in Fig. 1 of Section 3.2, we see that, as expected, in both the “preHiggs+ m_h ” and the “preHiggs+ m_h +hsig” distributions, light charginos and neutralinos are more preferred. The effect is more pronounced for the $\tilde{\chi}_1^\pm$ and $\tilde{\chi}_2^0$ than for the $\tilde{\chi}_1^0$. Note also that the preference for smaller μ through the Higgs signal strength measurements remains. Finally, note that the DM upper limits largely overrule the effect of the $c\tau$ cut: the red dashed line histograms are almost the same with or without the $c\tau$ cut. The exception is the $\tan\beta$ distribution. (The $\tilde{\chi}_1^0$, $\tilde{\chi}_2^0$, $\tilde{\chi}_1^\pm$ mass differences can however be smaller without the $c\tau$ cut.) The posterior densities of other quantities, which do not directly depend on M_1 , M_2 or μ show hardly any sensitivity to the $c\tau$ cut. In particular our conclusions about the Higgs signals remain unchanged.

It is of course also interesting to ask how likely it is at all to have a long-lived chargino. To this end we show in Fig. 9 the marginalized posterior density of the average $\tilde{\chi}_1^\pm$ lifetime. We find that the probability of $c\tau > 10$ mm is 28%, 25% and 47% at the “preHiggs+ m_h ”, “preHiggs+ m_h +hsig”, and “preHiggs+ m_h +hsig+DMup” levels, respectively.

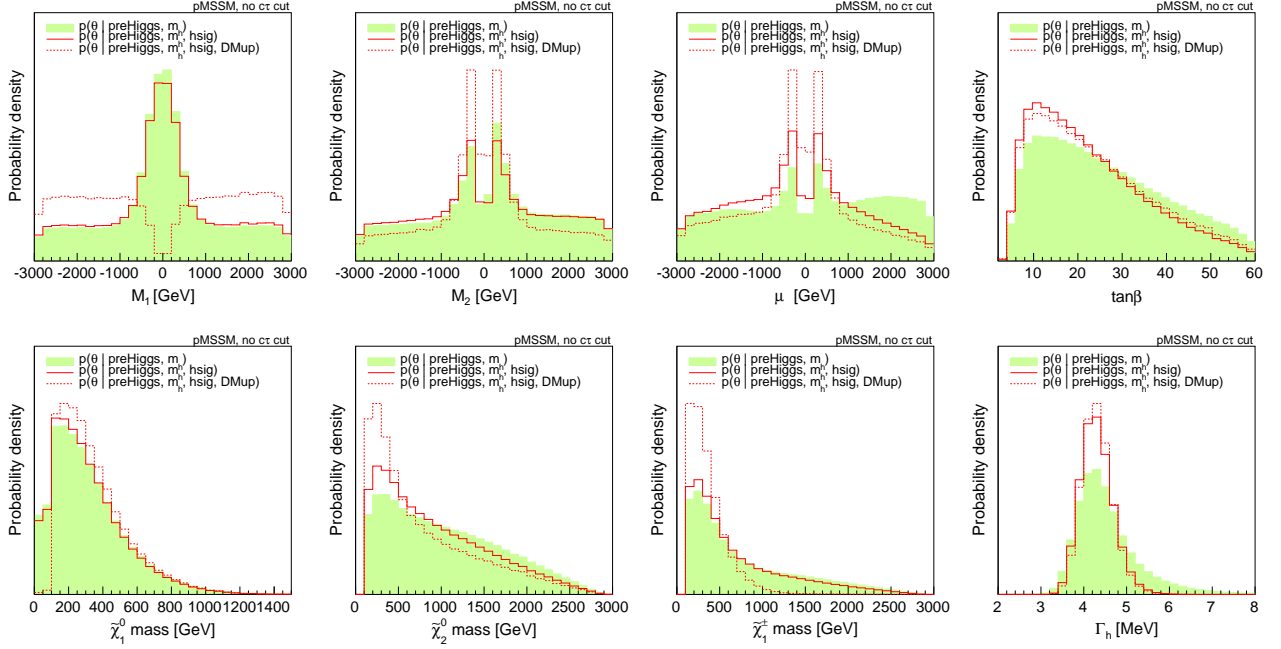


Figure 8: Marginalized 1D posterior densities for selected parameters and derived quantities without the prompt chargino requirement. The green histograms show the distributions based on the “preHiggs” measurements of Table 1 plus requiring in addition $m_h \in [123, 128]$ GeV, but without the $c\tau$ cut. The solid red lines are the distributions when taking into account in addition the measured Higgs signal strengths in the various channels, as well as the limits from the heavy MSSM Higgs searches. The dashed red lines include in addition an upper limit on the neutralino relic density and the recent direct DM detection limit from LUX.

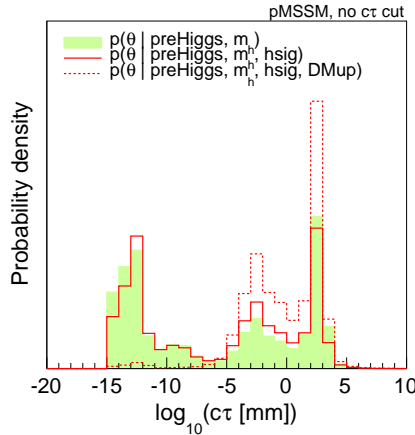


Figure 9: Marginalized 1D posterior density of the average $\tilde{\chi}_1^\pm$ lifetime, $c\tau$ in mm. Color codes as in Fig. 8.

3.4 Interplay with dark matter searches

As discussed above, the dark matter requirements (*i.e.*, imposing upper limits on the relic density and on the spin-independent scattering cross section) have a significant impact on the MSSM parameters and masses, and even on the h signal strengths. In this subsection, we now focus on dark matter observables themselves. Results for the neutralino relic density $\Omega_{\tilde{\chi}_1^0} h^2$ and the re-scaled spin-independent scattering cross section $\xi\sigma^{\text{SI}}(\tilde{\chi}_1^0 p)$ are shown in Figs. 10 and 11.

Let us start the discussion with the 1D distributions of $\log_{10}(\Omega_{\tilde{\chi}_1^0} h^2)$, shown in the upper row of plots in Fig. 10. Already the $p_0(\theta)$ distribution shows a two-peak structure with the minimum actually lying near the cosmologically preferred value $\Omega_{\tilde{\chi}_1^0} h^2 \approx 0.1$. This distribution is shifted to significantly higher values by the preHiggs constraints. Concretely, at preHiggs level, the probability for $\Omega_{\tilde{\chi}_1^0} h^2 < 0.14$ is 36% (53%) with (without) the prompt chargino requirement. This hardly changes when including also the requirement of $m_h = 123 - 128$ GeV: $p(\Omega_{\tilde{\chi}_1^0} h^2 < 0.14) \simeq 34\%$ (53%) in this case. The Higgs signal likelihood has a larger effect, shifting the distribution towards lower $\Omega_{\tilde{\chi}_1^0} h^2$. This is mainly due to the preference for smaller μ induced by the Higgs signal likelihood. The effect is thus less pronounced without the $c\tau$ cut (RH-side plot) than with the $c\tau$ cut (middle plot). Concretely, we find $p(\Omega_{\tilde{\chi}_1^0} h^2 < 0.14) \simeq 43\%$ (57%) with (without) the $c\tau$ cut. The peak at high $\Omega_{\tilde{\chi}_1^0} h^2$ values is of course completely removed by the DMup constraints. The probability of lying within the Planck window defined by $\Omega_{\tilde{\chi}_1^0} h^2 = 0.119 \pm 0.024$ (0.024 being the 2σ error, dominated by theory uncertainties) is, for all three of the above cases, $\sim 1.1\%$ with the $c\tau$ cut and $\sim 0.9\%$ without the $c\tau$ cut.

Turning to the predictions for direct dark matter detection, we observe that the preHiggs constraints limit the probability of having very small values of $\xi\sigma^{\text{SI}}(\tilde{\chi}_1^0 p)$. This is true with and without the $c\tau$ cut, though the effect is larger with the $c\tau$ cut. The latter is due to the fact that the prompt chargino requirement removes the pure wino-LSP scenarios which have extremely small $\Omega_{\tilde{\chi}_1^0} h^2$ and $\xi\sigma^{\text{SI}}(\tilde{\chi}_1^0 p)$ (recall that $\xi = \Omega_{\tilde{\chi}_1^0} h^2 / 0.119$). Requiring consistency with the Higgs signal strengths has only a small effect, somewhat preferring smaller values of $\xi\sigma^{\text{SI}}(\tilde{\chi}_1^0 p)$ because of the larger LSP higgsino component.

The 2D distributions of $\Omega_{\tilde{\chi}_1^0} h^2$ and $\xi\sigma^{\text{SI}}(\tilde{\chi}_1^0 p)$ versus the $\tilde{\chi}_1^0$ mass are shown in Fig. 11. We observe that on the one hand the neutralino LSP can have mass up to 1 TeV at 95% BC without conflicting with the DM constraints. Very low neutralino masses, on the other hand, are severely constrained by DM requirements. Note, moreover, that the most likely values lie around $m_{\tilde{\chi}_1^0} \approx 200\text{--}300$ GeV, $\Omega_{\tilde{\chi}_1^0} h^2 \approx 10^{-2}$ and $\xi\sigma^{\text{SI}}(\tilde{\chi}_1^0 p) \approx 10^{-10}$ pb.

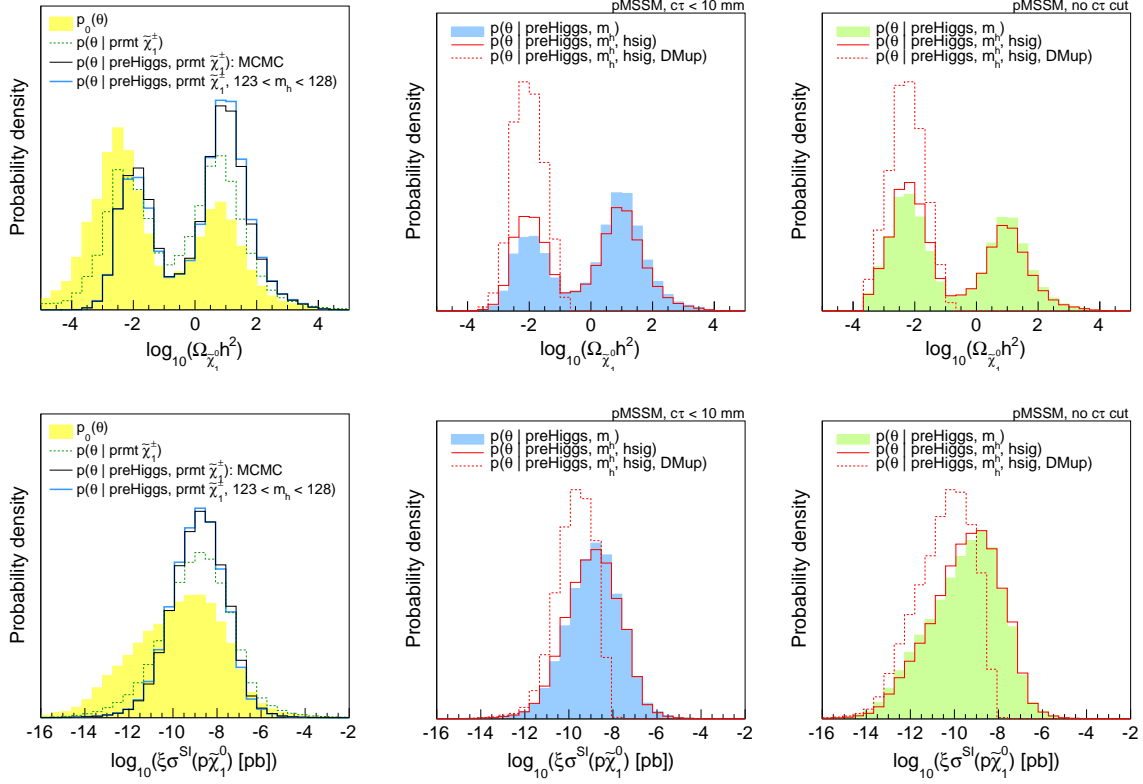


Figure 10: Marginalized 1D posterior densities for dark matter quantities. Color codes as in Fig. 1 (left), Fig. 3 (middle) and Fig. 8 (right).

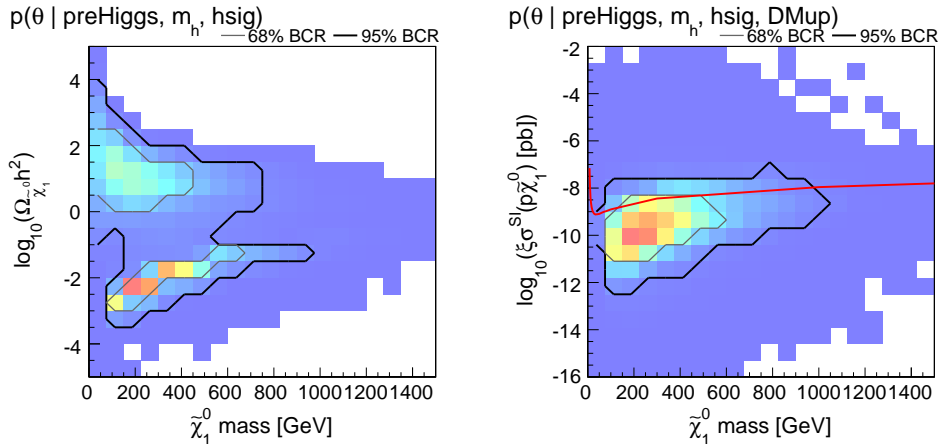


Figure 11: Marginalized 2D posterior densities for dark matter quantities. The probability density is represented by color shading, ranging from low values in blue to high values in red. The grey and black lines are contours of 68% and 95% Bayesian Credibility, respectively. The red line in the right plot is the 90% CL limit from LUX.

3.5 Consequences of future h signal strength measurements

It is also interesting to consider what happens if, with precision data at the next run of the LHC, the Higgs signal strengths have an even narrower probability distribution around unity. We estimate the precision attainable with 300 fb^{-1} at 14 TeV based on [50, 51]

$$\begin{aligned}
 \mu(\text{ggF} + \text{ttH}, \gamma\gamma) &= 1 \pm 0.1, & \mu(\text{VBF} + \text{VH}, \gamma\gamma) &= 1 \pm 0.3, \\
 \mu(\text{ggF} + \text{ttH}, VV) &= 1 \pm 0.1, & \mu(\text{VBF} + \text{VH}, VV) &= 1 \pm 0.6, \\
 \mu(\text{ggF} + \text{ttH}, b\bar{b}) &= 1 \pm 0.6, & \mu(\text{VBF} + \text{VH}, b\bar{b}) &= 1 \pm 0.2, \\
 \mu(\text{ggF} + \text{ttH}, \tau\tau) &= 1 \pm 0.2, & \mu(\text{VBF} + \text{VH}, \tau\tau) &= 1 \pm 0.2.
 \end{aligned}
 \tag{8}$$

The effect of these hypothetical results is illustrated in Fig. 12. We conclude that if the Higgs signal remains SM-like (but with smaller uncertainties), the effects already observed on some SUSY parameters are only slightly strengthened by more precise measurements.

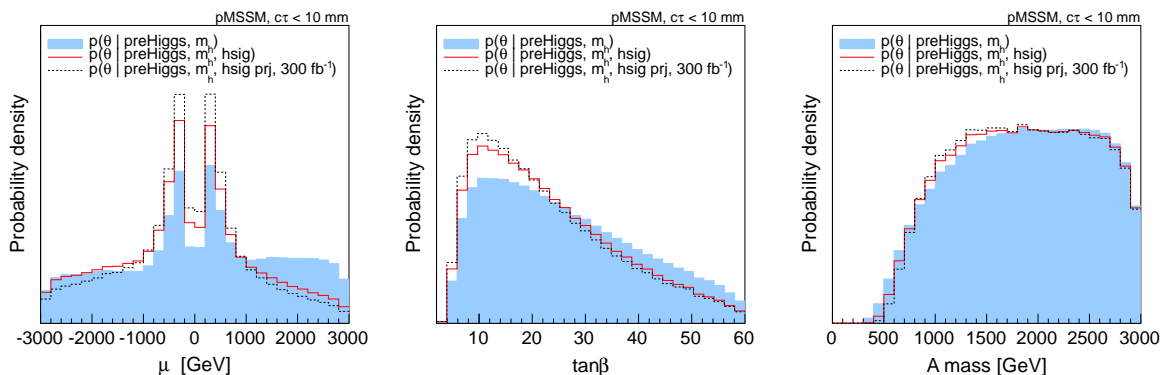


Figure 12: Marginalized 1D posterior densities for some MSSM parameters, showing the effect of all h signal strengths being ≈ 1 with uncertainties as expected for 300 fb^{-1} of data at 14 TeV, *cf.* Eq. (8).

The picture is quite different should the signal strength finally turn out to be larger than one. For illustration, we assume $\mu(\text{ggF}, \gamma\gamma) > 1$ and show in Fig. 13 the impact on some other quantities. As we have seen, $\Delta_b < 0$ corresponds to a suppression of $h \rightarrow b\bar{b}$ and, hence, to the enhancement of all other signal strengths. This is how one obtains $\mu(\text{ggF}, \gamma\gamma) > 1$ in our case. This leads to a strong preference for $\mu < 0$ and to an associated asymmetry for the M_2 distribution. Moreover, strong evidence for $\mu(\text{ggF}, \gamma\gamma) > 1$ would strongly disfavor a CP-odd Higgs lying close to the current CMS bound because of the impact of m_A on the tree-level coupling hbb . Finally, $\mu(\text{ggF}, \gamma\gamma) > 1$ would also imply a preference for an enhancement of the diphoton signal in VBF production, as well as an enhancement of the ZZ mode in both

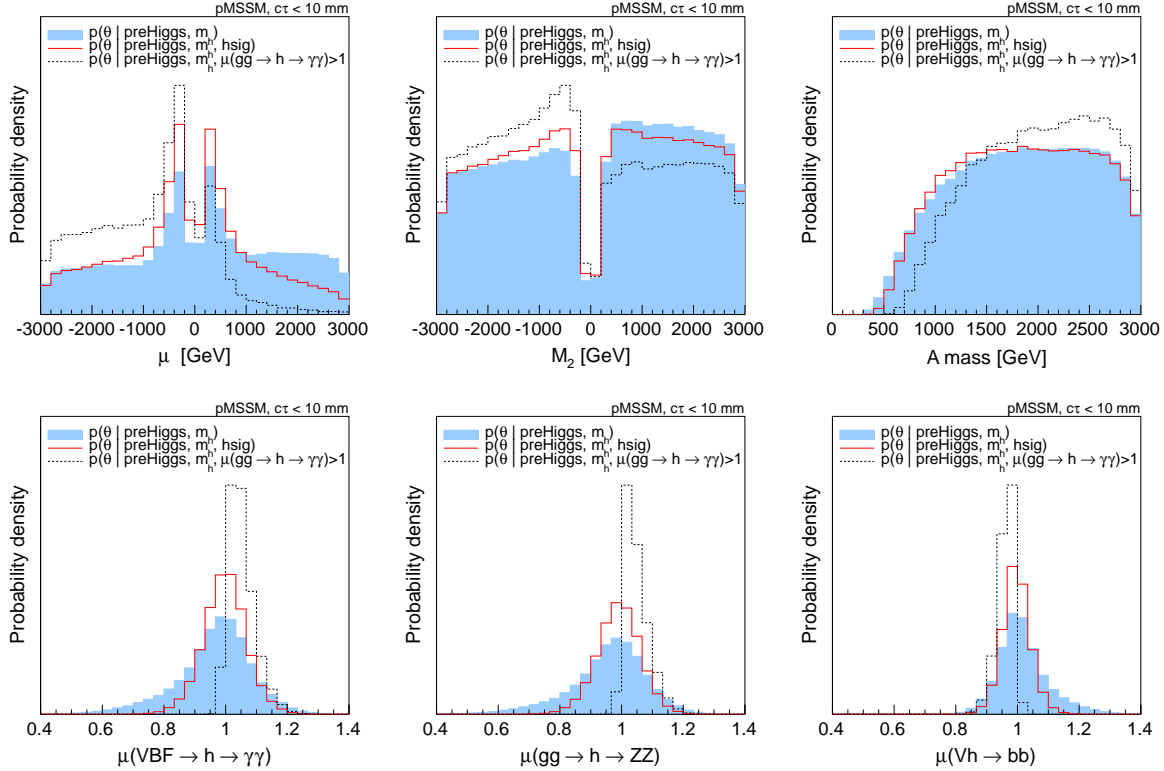


Figure 13: Marginalized 1D posterior densities for selected MSSM parameters and h signal strengths, showing the effect of a hypothetical future determination of $\mu(gg \rightarrow h \rightarrow \gamma\gamma) > 1$.

ggF and VBF. This is accompanied at the same time by the expected suppression of $Vh \rightarrow b\bar{b}$. Nonetheless, signal strength values close to 1 are still the most likely ones.

4 Conclusions

We have performed a Bayesian analysis of the pMSSM taking into account the latest LHC results on the Higgs signal at 125.5 GeV in addition to relevant low-energy observables and LEP constraints. We find that the requirement of obtaining the right m_h strongly favors $|X_t/M_{\text{SUSY}}| \approx 2$, *i.e.* near-maximal (but not maximal) stop mixing. Coincidentally, such near-maximal mixing is also favored by naturalness arguments [46].

The constraints from the Higgs signal strengths in the various production \times decay modes, on the other hand, have an important influence on the posterior distributions of μ and $\tan\beta$, and hence on the electroweak-ino spectrum. Concretely, low values of μ and $\tan\beta \approx 10$ are favored. This is mainly due to radiative corrections to the bottom Yukawa coupling, which are proportional to $\mu \tan\beta$ and can significantly modify the total Higgs width. As a consequence,

$\tilde{\chi}_2^0$ and $\tilde{\chi}_1^\pm$ masses below about 500 GeV are favored, as are LSPs with a significant higgsino fraction. While there is of course still a substantial tail at large masses, these results suggest that the Higgs data yield a certain preference for natural-SUSY-like scenarios.

Regarding the heavy Higgs states, H and A , we find that $m_{H,A} \gtrsim 500$ GeV mostly due to B-physics constraints. The 125 GeV Higgs data give only a small additional constraint; they mostly affect the heavy Higgses through their effect on $\tan\beta$. The limits from direct searches for $H, A \rightarrow \tau\tau$ at 7–8 TeV are less sensitive. If $m_A \lesssim 1$ TeV, prospects for discovery of H and A at the next LHC run are substantial. Because $\tan\beta \gtrsim 10$ is preferred, we find that $b\bar{b} \rightarrow H, A$ typically dominates (by about a factor of 30) over gluon fusion, with $\sigma(b\bar{b} \rightarrow H, A)\text{BR}(H, A \rightarrow \tau\tau)$ of the order of a few fb.

We have also explored the impact of DM limits associated with $\Omega_{\tilde{\chi}_1^0} h^2$ and $\xi\sigma^{\text{SI}}(\tilde{\chi}_1^0 p)$ on the Higgs bosons in the pMSSM context as well as the impact of the Higgs precision data on these same DM observables. The most probable values for $\Omega_{\tilde{\chi}_1^0} h^2$ lie in the vicinity of 10^{-2} , implying that DM would not consist entirely of the $\tilde{\chi}_1^0$ (or that the missing abundance of $\tilde{\chi}_1^0$ is substituted by non-thermal production). The probability for obtaining $\Omega_{\tilde{\chi}_1^0} h^2$ within the Planck window is only of order 1%: to get the correct annihilation rate, the $\tilde{\chi}_1^0$ has to have a carefully balanced composition, or a mass that is fine-tuned with respect to the A or co-annihilating sparticles. Imposing the upper limit on $\Omega_{\tilde{\chi}_1^0} h^2$, we find $m_{\tilde{\chi}_1^0} \in [100, 760]$ GeV and $\xi\sigma^{\text{SI}}(\tilde{\chi}_1^0 p) \gtrsim 3.5 \times 10^{-12}$ pb at 95% BC.

While we have not taken into account the recent LHC limits from direct SUSY searches, we have checked that our conclusions do not change when requiring gluino and squark masses above 1 TeV. The conclusions drawn from the Higgs sector are thus orthogonal to those from the SUSY searches. In particular, this makes our results directly comparable to the pMSSM interpretation of the CMS SUSY searches at 7–8 TeV [18, 19].

The 13–14 TeV run of the LHC will provide increased precision for Higgs measurements as well as a higher reach for SUSY particles. Particularly relevant in point of view of an interplay between Higgs and SUSY results is an improved sensitivity for higgsinos, gluinos and 3rd generation squarks. It will be interesting to see if a tension between Higgs results and SUSY limits arises or if there is a convergence as a result of the discovery of, *e.g.*, light charginos and neutralinos. Last but not least, if the Higgs boson is found in the end to have an enhanced $h \rightarrow \gamma\gamma$ rate compared to the SM, implications for μ and M_2 are substantial, m_A is shifted to higher values and $\mu(Vh \rightarrow Vb\bar{b})$ is suppressed — allowing for some possibility of verifying consistency with or creating tension within the pMSSM.

5 Acknowledgements

We are deeply indebted to Sezen Sekmen for her extensive and crucial contributions during the first part of the project. Without her, this work would not have been possible. We strongly acknowledge her collaboration.

This work was supported in part by the US DOE grant DE-FG03-91ER40674 and by IN2P3 under contract PICS FR–USA No. 5872. J.F.G. and S.K. also thank the Aspen Center for Physics, supported by the National Science Foundation under Grant No. PHYS-1066293, for hospitality and a great working atmosphere.

References

- [1] **ATLAS** Collaboration, G. Aad *et al.*, “Observation of a new particle in the search for the Standard Model Higgs boson with the ATLAS detector at the LHC,” *Phys.Lett.* **B716** (2012) 1–29, 1207.7214.
- [2] **CMS** Collaboration, S. Chatrchyan *et al.*, “Observation of a new boson at a mass of 125 GeV with the CMS experiment at the LHC,” *Phys.Lett.* **B716** (2012) 30–61, 1207.7235.
- [3] **ATLAS** Collaboration, G. Aad *et al.*, “Measurements of Higgs boson production and couplings in diboson final states with the ATLAS detector at the LHC,” *Phys.Lett.* **B726** (2013) 88–119, 1307.1427.
- [4] **ATLAS** Collaboration, “Combined measurements of the mass and signal strength of the Higgs-like boson with the ATLAS detector using up to 25 fb⁻¹ of proton-proton collision data,” Tech. Rep. ATLAS-CONF-2013-014, CERN, Geneva, Mar, 2013.
- [5] **CMS** Collaboration, “Combination of standard model Higgs boson searches and measurements of the properties of the new boson with a mass near 125 GeV,” Tech. Rep. CMS-PAS-HIG-13-005, CERN, Geneva, 2013.
- [6] G. Belanger, B. Dumont, U. Ellwanger, J. Gunion, and S. Kraml, “Global fit to Higgs signal strengths and couplings and implications for extended Higgs sectors,” *Phys.Rev.* **D88** (2013) 075008, 1306.2941.
- [7] S. P. Martin, “A Supersymmetry primer,” hep-ph/9709356.
- [8] D. Chung, L. Everett, G. Kane, S. King, J. D. Lykken, *et al.*, “The Soft supersymmetry breaking Lagrangian: Theory and applications,” *Phys.Rept.* **407** (2005) 1–203, hep-ph/0312378.
- [9] M. Carena, S. Gori, N. R. Shah, C. E. Wagner, and L.-T. Wang, “Light Stau Phenomenology and the Higgs $\gamma\gamma$ Rate,” *JHEP* **1207** (2012) 175, 1205.5842.

- [10] U. Ellwanger, “A Higgs boson near 125 GeV with enhanced di-photon signal in the NMSSM,” *JHEP* **1203** (2012) 044, 1112.3548.
- [11] J. F. Gunion, Y. Jiang, and S. Kraml, “The Constrained NMSSM and Higgs near 125 GeV,” *Phys.Lett.* **B710** (2012) 454–459, 1201.0982.
- [12] S. Kraml, “Implications of LHC Higgs results for supersymmetry,” *J.Phys.Conf.Ser.* **455** (2013) 012053.
- [13] A. Arbey, M. Battaglia, A. Djouadi, and F. Mahmoudi, “An update on the constraints on the phenomenological MSSM from the new LHC Higgs results,” *Phys.Lett.* **B720** (2013) 153–160, 1211.4004.
- [14] A. Djouadi, L. Maiani, G. Moreau, A. Polosa, J. Quevillon, *et al.*, “The post-Higgs MSSM scenario: Habemus MSSM?,” 1307.5205.
- [15] M. Cahill-Rowley, J. Hewett, A. Ismail, and T. Rizzo, “Constraints on Higgs Properties and SUSY Partners in the pMSSM,” 1308.0297.
- [16] **LHC Higgs Cross Section Working Group** Collaboration, S. Heinemeyer *et al.*, “Handbook of LHC Higgs Cross Sections: 3. Higgs Properties,” 1307.1347.
- [17] F. Boudjema, G. Cacciapaglia, K. Cranmer, G. Dissertori, A. Deandrea, *et al.*, “On the presentation of the LHC Higgs Results,” 1307.5865.
- [18] **CMS** Collaboration, “Phenomenological MSSM interpretation of the CMS results at $\sqrt{s}=7$ TeV,” Tech. Rep. CMS-PAS-SUS-12-030, 2012.
- [19] **CMS** Collaboration, “Phenomenological MSSM interpretation of the CMS 2011 and 2012 results,” Tech. Rep. SUS-13-020, 2013. in preparation.
- [20] **MSSM Working Group** Collaboration, A. Djouadi *et al.*, “The Minimal supersymmetric standard model: Group summary report,” hep-ph/9901246.
- [21] J. Camargo-Molina, B. O’Leary, W. Porod, and F. Staub, “**Vevacious**: A Tool For Finding The Global Minima Of One-Loop Effective Potentials With Many Scalars,” *Eur.Phys.J.* **C73** (2013) 2588, 1307.1477.
- [22] B. Allanach, “SOFTSUSY: a program for calculating supersymmetric spectra,” *Comput.Phys.Commun.* **143** (2002) 305–331, hep-ph/0104145.
- [23] F. Mahmoudi, “SuperIso v2.3: A Program for calculating flavor physics observables in Supersymmetry,” *Comput.Phys.Commun.* **180** (2009) 1579–1613, 0808.3144.
- [24] G. Belanger, F. Boudjema, A. Pukhov, and A. Semenov, “MicrOMEGAs: A Program for calculating the relic density in the MSSM,” *Comput.Phys.Commun.* **149** (2002) 103–120, hep-ph/0112278.

- [25] M. Muhlleitner, A. Djouadi, and Y. Mambrini, “SDECAY: A Fortran code for the decays of the supersymmetric particles in the MSSM,” *Comput.Phys.Commun.* **168** (2005) 46–70, [hep-ph/0311167](#).
- [26] A. Djouadi, J. Kalinowski, and M. Spira, “HDECAY: A Program for Higgs boson decays in the standard model and its supersymmetric extension,” *Comput.Phys.Commun.* **108** (1998) 56–74, [hep-ph/9704448](#).
- [27] P. Z. Skands, B. Allanach, H. Baer, C. Balazs, G. Belanger, *et al.*, “SUSY Les Houches accord: Interfacing SUSY spectrum calculators, decay packages, and event generators,” *JHEP* **0407** (2004) 036, [hep-ph/0311123](#).
- [28] **Heavy Flavor Averaging Group** Collaboration, Y. Amhis *et al.*, “Averages of B-Hadron, C-Hadron, and tau-lepton properties as of early 2012,” [1207.1158](#).
- [29] M. Misiak, H. Asatrian, K. Bieri, M. Czakon, A. Czarnecki, *et al.*, “Estimate of $\mathcal{B}(\bar{B} \rightarrow X_s \gamma)$ at $\mathcal{O}(\alpha_s^2)$,” *Phys.Rev.Lett.* **98** (2007) 022002, [hep-ph/0609232](#).
- [30] **Heavy Flavor Averaging Group** Collaboration, Y. Amhis *et al.*, “HFAG update, May 2013.”
<http://www.slac.stanford.edu/xorg/hfag/rare/2013/radll/OUTPUT/TABLES/radll.pdf>.
- [31] **ATLAS, CMS and LHCb** Collaboration, “Search for the rare decays Bs and B0 to dimuons at the LHC with the ATLAS, CMS and LHCb experiments,” tech. rep., 2012.
- [32] **CMS and LHCb** Collaboration, “Combination of results on the rare decays $B_s^0 \rightarrow \mu^+ \mu^-$ from the CMS and LHCb experiments,” tech. rep., 2013.
- [33] **Particle Data Group** Collaboration, K. Nakamura *et al.*, “Review of particle physics,” *J.Phys.* **G37** (2010) 075021.
- [34] K. Hagiwara, R. Liao, A. D. Martin, D. Nomura, and T. Teubner, “ $(g - 2)_\mu$ and $\alpha(M_Z^2)$ re-evaluated using new precise data,” *J.Phys.* **G38** (2011) 085003, [1105.3149](#).
- [35] **ATLAS and CMS** Collaboration, “Combination of ATLAS and CMS results on the mass of the top quark using up to 4.9 fb^{-1} of data,” tech. rep., 2012.
- [36] **Tevatron Electroweak Working Group, CDF and D0 Collaborations** Collaboration, M. Muether *et al.*, “Combination of CDF and DO results on the mass of the top quark using up to 8.7 fb^{-1} at the Tevatron,” [1305.3929](#).
- [37] LEPSUSYWG, ALEPH, DELPHI, L3 and OPAL experiments. notes
LEPSUSYWG/01-03.1, LEPSUSYWG/02-04.1, and LEPSUSYWG/04-01.1,
<http://lepsusy.web.cern.ch/lepsusy/Welcome.html>.
- [38] R. Trotta, “Bayes in the sky: Bayesian inference and model selection in cosmology,” *Contemp.Phys.* **49** (2008) 71–104, [0803.4089](#).

- [39] **LHCb** Collaboration, R. Aaij *et al.*, “First Evidence for the Decay $B_s^0 \rightarrow \mu^+ \mu^-$,” *Phys.Rev.Lett.* **110** (2013) 021801, 1211.2674.
- [40] **CMS** Collaboration, “Higgs to tau tau (MSSM),” Tech. Rep. CMS-PAS-HIG-13-021, CERN, Geneva, 2013.
- [41] **Planck** Collaboration, P. Ade *et al.*, “Planck 2013 results. XVI. Cosmological parameters,” 1303.5076.
- [42] **LUX** Collaboration, D. Akerib *et al.*, “First results from the LUX dark matter experiment at the Sanford Underground Research Facility,” 1310.8214.
- [43] J. F. Gunion and H. E. Haber, “Two-body decays of neutralinos and charginos,” *Phys.Rev.* **D37** (1988) 2515.
- [44] A. Djouadi, “The Anatomy of electro-weak symmetry breaking. II. The Higgs bosons in the minimal supersymmetric model,” *Phys.Rept.* **459** (2008) 1–241, hep-ph/0503173.
- [45] F. Brummer, S. Kraml, and S. Kulkarni, “Anatomy of maximal stop mixing in the MSSM,” *JHEP* **1208** (2012) 089, 1204.5977.
- [46] C. Wymant, “Optimising Stop Naturalness,” *Phys.Rev.* **D86** (2012) 115023, 1208.1737.
- [47] M. S. Carena, D. Garcia, U. Nierste, and C. E. Wagner, “Effective Lagrangian for the $\bar{t}bH^+$ interaction in the MSSM and charged Higgs phenomenology,” *Nucl.Phys.* **B577** (2000) 88–120, hep-ph/9912516.
- [48] H. Eberl, K. Hidaka, S. Kraml, W. Majerotto, and Y. Yamada, “Improved SUSY QCD corrections to Higgs boson decays into quarks and squarks,” *Phys.Rev.* **D62** (2000) 055006, hep-ph/9912463.
- [49] R. V. Harlander, S. Liebler, and H. Mantler, “SusHi: A program for the calculation of Higgs production in gluon fusion and bottom-quark annihilation in the Standard Model and the MSSM,” *Computer Physics Communications* **184** (2013) 1605–1617, 1212.3249.
- [50] **ATLAS** Collaboration, “Physics at a High-Luminosity LHC with ATLAS (Update),” Tech. Rep. ATL-PHYS-PUB-2012-004, CERN, Geneva, Oct, 2012.
- [51] **CMS** Collaboration, “CMS at the High-Energy Frontier. Contribution to the Update of the European Strategy for Particle Physics,” Tech. Rep. CMS-NOTE-2012-006. CERN, Geneva, Oct, 2012.